# Nanoscale

Accepted Manuscript


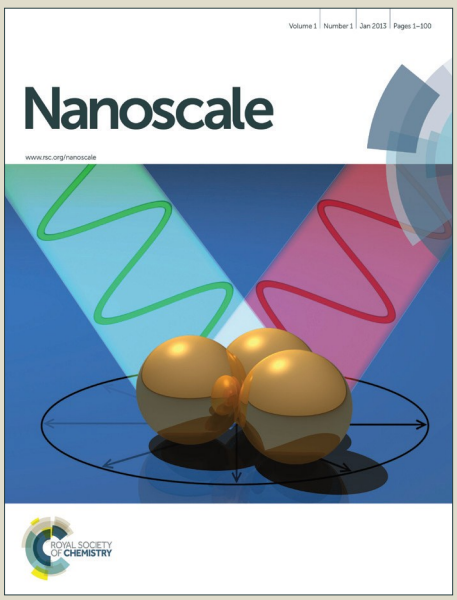





ROYAL SOCIETY OF CHEMISTRY

www.rsc.org/nanoscale

# Tuning upconversion through a sensitizer/activator-isolated $NaYF_4$ core/shell structure

Shuai Ye,[1,2] Guanying Chen,*[2,3] Wei Shao, [2,3] Junle Qu,*[1,2] Paras N. Prasad*[2,4]

[1]Key Laboratory of Optoelectronic Devices and Systems of Guangdong Province, College of Optoelectronic Engineering, Shenzhen University, Shenzhen, 518060, People's Republic of China

[2]Institute for Lasers, Photonics, and Biophotonics, University at Buffalo, State University of New York, Buffalo, New York 14260, United States

[3]School of Chemical Engineering and Technology, Harbin Institute of Technology, Harbin, Heilongjiang 150001, People's Republic of China

[4]Department of Chemistry, Korea University, Seoul 136-701, Korea

*Email: chenguanying@hit.edu.cn, jlqu@szu.edu.cn, pnprasad@buffalo.edu

## Abstract

The ability to tune the emission color of upconversion nanoparticles (UCNPs) will greatly enhance the scope of their applications, ranging from infrared solar cells to volumetric multiplexed bioimaging. Conventional methods to tune upconversion are to vary the type and/or the concentration of doped rare-earth ions in these nanoparticle formulations. Here, we introduce a different approach to vary the emission colors of the frequently used sensitizer/activator pairs of $Yb^{3+}/RE^{3+}$ (RE=Ho, Er, Tm) via utilization of a sensitizer/activator-isolated $NaYF_4$ core-shell structure. We show that the typical green, yellow, and blue luminescent colors from $Yb^{3+}/Ho^{3+}$-, $Yb^{3+}/Er^{3+}$-, and $Yb^{3+}/Tm^{3+}$-co-doped $NaYF_4$ UCNPs can be converted into the quasi-white, green, and pink blue, when corresponding core-shell structures of $NaYF_4$:$Yb^{3+}$ @$NaYF_4$:$Ho^{3+}$, $NaYF_4$:$Yb^{3+}$ @$NaYF_4$:$Er^{3+}$and $NaYF_4$:$Yb^{3+}$ @$NaYF_4$:$Tm^{3+}$ are built. Time-resolved spectra indicate that decay lifetimes of the emission bands from the sensitizer/activator-isolated core-shell structure significantly vary from that of the sensitizer/activator-codoped $NaYF_4$ UCNPs, verifying the strain-induced modulation of emission channels in the core-shell structure. These sensitizer-activator-isolated core-shell UCNPs have implications for a range of biophotonic or photonic applications.

## Introduction

Rare-earth-doped upconversion nanoparticles (UCNPs) are receiving a great deal of attention due to their captivating photon upconverting ability whereby near-infrared long-wavelength excitation at very low power can be converted into shorter wavelength emissions [1-5]. Along with the asset of nanometer dimension and low toxicity, this frequency ability allows UCNPs to be utilized for a broad spectrum of applications such as, bioimaging, biosensing, solar cells, optical data storage, drug delivery, and light-activated therapy, etc [6-12]. However, most of these applications require the ability to tune the upconversion color to meet the need of a specific application [13,14]. For example, a set of colors are needed to pinpoint a range of organelles in a single cell to unravel the biological complexity behind or to entail a high throughput screening to detect disease markers in a blood drop [15].

The typically used UCNPs are $NaYF_4$ nanoparticles doped with the sensitizer/activator ion pairs of $Yb^{3+}/RE^{3+}$ (RE=Er, Tm, Ho), as these UCNPs have been known to be one of the most efficient UC systems up to date [16,17]. Each trivalent lanthanide activator $X^{3+}$ has a unique energy level structure to produce emission peaks at specific wavelengths even in different host materials of varying size. This restricts the tunability of the luminescence color output as found in quantum dots exhibiting size-dependent color tunability due to quantum confinement effect [18]. However, the excitation and relaxation dynamics of energy levels involved in upconversion processes can be manipulated to vary the relative luminescence intensity between different UC bands of a lanthanide ion or to realize a combination of UC emission bands from different lanthanide ions, thus providing routes to tune the resulting color output from UCNPs [19-25]. Indeed, a common method in literature to tune upconversion is to select a combination of activators or to vary the concentration of the sensitizer $Yb^{3+}$ ions and/or the activator ion concentrations. Zhang *et al.* reported on incorporation of two or more activators ions into the core $NaYF_4$ nanoparticle or the shell on it to produce different color output [26,27]. Liu *et al.* reported on fine tuning the color output of $Yb^{3+}/Er^{3+}$ and/or $Yb^{3+}/Tm^{3+}$ codoped $NaYF_4$ nanoparticles through variation of the concentrations of the $Yb^{3+}$, $Tm^{3+}$, or $Er^{3+}$ ions [28]. Moreover, the UC emission color from a single lanthanide activator was also varied through modulating the relative intensity between different emission bands by

incorporating other ions (such as $Mn^{2+}$, $Zr^{4+}$ , $Ce^{3+}$ions) into the same nanoparticles to introduce ion-ion interaction [29-34], or by size-, shape- or ligand-dependent surface-related nonradiative processes, to manipulate the energy transfer pathways [35-38]. However, none of these methods are able to engineer optical selection routes to tune the UC color output. Here, we introduce an approach to tune upconversion through strain-induced modulation of optical parameters of $RE^{3+}$ in the $NaYF_4$:$Yb^{3+}$ @$NaYF_4$:$RE^{3+}$ (RE=Ho, Er, Tm) core-shell structure, which yields a quite different color output from that of the corresponding $NaYF_4$:$Yb^{3+}$/$RE^{3+}$ UCNPs.

## Experimental

2.1 Synthesis of $NaYF_4$:$Yb^{3+}$/$RE^{3+}$ (RE=Ho, Er, Tm) nanoparticles with varied $Yb^{3+}$ and $RE^{3+}$ concentrations

All chemical materials were purchased from Sigma-Aldrich and used without further purification. The employed rare-earth chloride hexdydrates have a rare-earth trace metal basis of 99.9%. The $NaYF_4$ nanoparticles doped with 100x% $Yb^{3+}$ ions (x=0.2, 0.4, 0.5, 0.99) and 100y% $RE^{3+}$ ions (y=0.01) were synthesized through a modified procedure in literature [39,40]. Typically, x mmol $YbCl_3.6H_2O$, y mmol $RECl_3.6H_2O$, and 1-x-y mmol of $YCl_3.6H_2O$ were firstly added into a 100 ml three-necked round bottom flask which was then loaded with 7 ml oleic acid and 15 ml 1-octadecene. The mixture was then heated at 160$^oC$ under argon atmosphere protection for 60 min under vigorous stirring. After cooling down to room temperature, 10 ml methanol containing 4 mmol of $NH_4F$ and 2.5 mmol of NaOH was added into the flask. After evaporating methanol, the mixture solution was heated to 300 $^oC$ under Ar atmosphere for 60 min and then cooled to room temperature. The UCNPs were precipitated and collected by adding ethanol, followed by centrifugation at 8000 rmp. These conventional UCNPs were dispersed in 10 ml hexane for later use.

2.2 Synthesis of core/shell $NaYF_4$:$Yb^{3+}$@$NaYF_4$:$RE^{3+}$ (RE=Ho, Er, Tm) nanoparticles with varied concentration of $Yb^{3+}$ and $RE^{3+}$ ions.

To prepare the core-shell $NaYF_4$:100x%$Yb^{3+}$@$NaYF_4$:100y% $RE^{3+}$ (RE=Ho, Er, Tm) UCNPs , 1 mmol core nanoparticles of $NaYF_4$ doped with 100x%$Yb^{3+}$ ion concentration were

firstly prepared following the procedure described in 2.1. Then, y mmol $RECl_3.6H_2O$ and 1-y mmol of $YCl_3.6H_2O$ were added into a 100 ml flask which contained 7 ml oleic acid and 15 ml of 1-octadecene. Subsequently, the solution was heated at 160$^o$C for 60 min under Ar atmosphere with vigorous stirring, which was then cooled to room temperature. The pre-prepared core $NaYF_4$:100x%$Yb^{3+}$ nanoparticles dispersed in 10 mL hexane and a 4 mmol of $NH_4F$ and 2.5 mmol of NaOH solved in 10 ml methanol were both added into this solution. After removal of methanol via evaporation, the solution was heated to 300$^o$C under Ar atmosphere for 60 min, and finally cooled to room temperature. The core-shell $NaYF_4$:100x%$Yb^{3+}$@$NaYF_4$:100y% $RE^{3+}$ nanoparticles were precipitated with ethanol and collected via centrifugation at 8000 rmp. After washing several times with ethanol, they were then dispersed in 10 ml hexane for characterizations.

2.3 Characterization

The size and morphology of the nanoparticles were characterized by transmission electron microscopy (TEM) using a JEM-2010 microscope at an acceleration voltage of 200 KV. The element concentrations of the resulting nanoparticles were evaluated with single quadrupole mass spectrometer with inductively coupled plasma source (Thermo Scientific XSERIES 2 ICPMS). The UC luminescence spectra were recorded using a Fluorolog-3.11 Jobin Yvon spectrofluorometer with a slit width defining spectral resolution of 2 nm. The colloidal UCNPs were excited at ~980 nm using a fiber-coupled laser diode (Q-Photonics). Photographic images of UC emissions were taken by a digital camera of Canon D600. The decays of the UC emissions at 545 and 650 nm from $Ho^{3+}$ ions, and at 545 and 655 nm from $Er^{3+}$ ions were recorded at the Infinium oscilloscope (Hewlett-Packard) coupled to the PMT of Fluorolog-3.11 Jobin Yvon spectrofluorometer, employing the excitation by nanosecond pulsed laser of 532 nm (second harmonic, Nd:YAG) at a repetition rate of 20 Hz. With respect to the decays of the UC emissions at 478, 650, and 800 nm from $Tm^{3+}$ ions, the third harmonic laser output from Nd:YAG laser at 355 nm was utilized for excitation. For all luminescence spectra and decay measurements, the emission signal of the sample (dispersed in hexane) in a cuvette was collected at 90 °relative to the excitation beam.

## Results and discussions

To investigate the upconversion luminescence tuning of $NaYF_4:Yb^{3+}$ @$NaYF_4:X^{3+}$ (X=Ho, Er, Tm) core/shell nanoparticles as compared to $NaYF_4:Yb^{3+}/X^{3+}$, we first selected X=Ho as a starting point and prepared a set of $NaYF_4:Yb^{3+}$x%@$NaYF_4$: $Ho^{3+}$ 1% core-shell and conventional $NaYF_4:Yb^{3+}$x%, $Ho^{3+}$ 1% UCNPs (Figure 1, TEM images). All the conventional and core-shell nanoparticles are very uniform in shape and size. The shape and size of the conventional $NaYF_4:Yb^{3+}$x%, $Ho^{3+}$ 1% core UCNPs are dependent on the $Yb^{3+}$ concentration, yielding a similar dependence for the $NaYF_4:Yb^{3+}$x%@$NaYF_4$: $Ho^{3+}$ 1% core-shell UCNPs. The nanospheres of the conventional UCNPs at $Yb^{3+}$ of 20% were converted into hexagons both at $Yb^{3+}$ concentrations of 40, and 50%. Correspondingly, rod-like core-shell UCNPs are transformed into hexagons when $Yb^{3+}$ concentration reaches 40 and 50%. The average size of the conventional UCNPs at $Yb^{3+}$ concentrations of 20, 40, and 50% was evaluated to be ~20, 33, and 56 nm, while the core-shell UCNPs accordingly have a size of ~23, ~40, and 58 nm, respectively. This corresponds to a uniform shell thickness of ~ 1.5-3.5 nm. Interestingly, a core-shell structure can be clearly discerned in Figure 1 c owing to an adequate high concentration of $Yb^{3+}$ ions in the core to create a good phase contrast from the shell material that contains a large amount of $Y^{3+}$ ions. This is consistent with our previous observation [41]. In addition, selected-area electron diffraction patterns of the core-shell and the conventional UCNPs confirmed that both nanoparticles are hexagonal having crystallgraphic phases to the standard hexagonal $NaYF_4$ host lattice of JCPDS 28-1192 (Supporting Information, Figure S1). We also prepared the core/shell UCNPs with higher $Yb^{3+}$ concentrations at 60 and 80%; however, two quite different size nanoparticles appear, possibly owing to the self-nucleation of the shell materials (Supporting Information, Figure S2). We intended to omit the discussion of these materials for the reason of clarity, except using their luminescence data in Figure 2 (d).

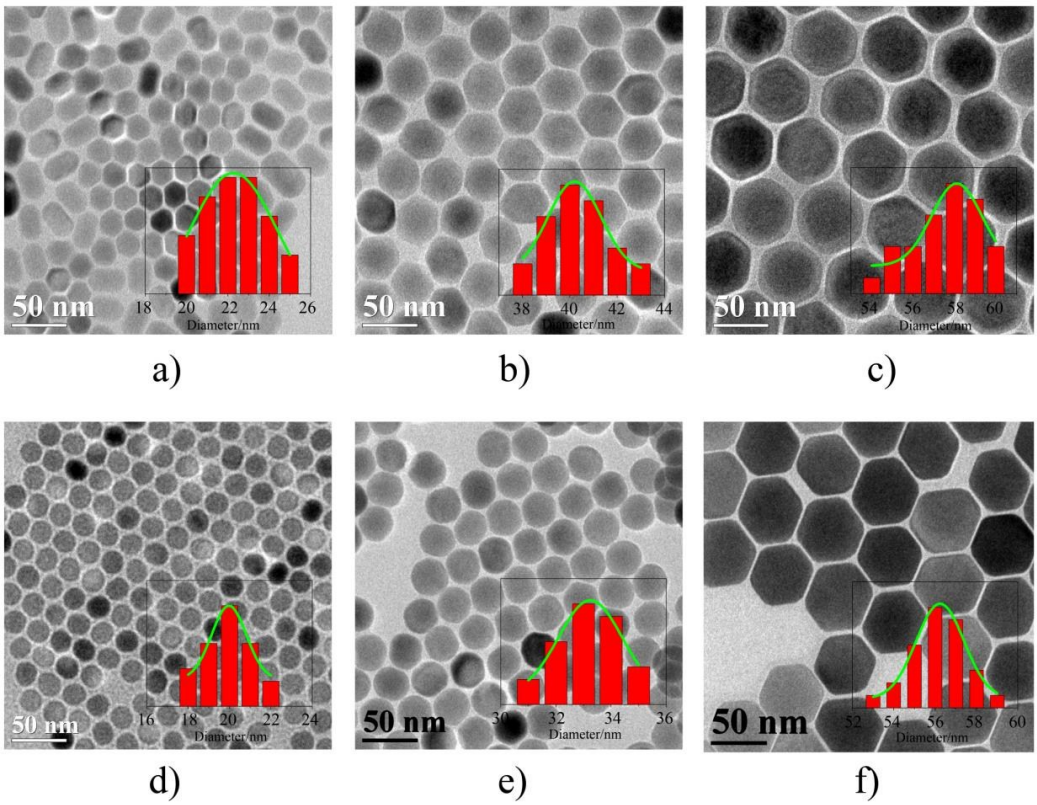


**Figure 1.** TEM micrographic images of the core/shell UCNPs of a) $NaYF_4$:$Yb^{3+}$20%@$NaYF_4$:$Ho^{3+}$1%, b) $NaYF_4$:$Yb^{3+}$40%@$NaYF_4$:$Ho^{3+}$1%, c) $NaYF_4$:$Yb^{3+}$50%@$NaYF_4$:$Ho^{3+}$1%, and the conventional UCNPs of d) $NaYF_4$:$Yb^{3+}$20%,$Ho^{3+}$1%, e) $NaYF_4$:$Yb^{3+}$40%,$Ho^{3+}$1%, f) $NaYF_4$:$Yb^{3+}$50%,$Ho^{3+}$1%

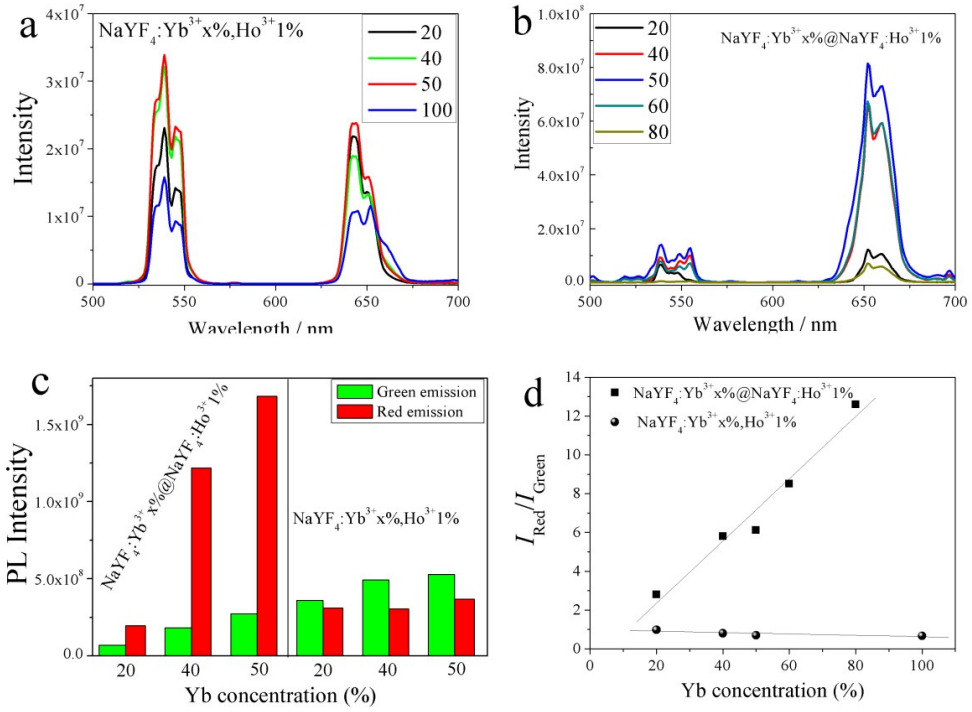


**Figure 2.** Photoluminescence spectra of (a) $NaYF_4$:$Yb^{3+}$x%,$Ho^{3+}$1% nanoparticles (x=20, 40, 50, 100) and (b)$NaYF_4$:$Yb^{3+}$x%@$NaYF_4$:$Ho^{3+}$1% nanoparticles (x=20, 40, 60, 80); (c) Photoluminescence intensity of the green and red emission band from $NaYF_4$:$Yb^{3+}$x%@$NaYF_4$:$Ho^{3+}$1% nanoparticles and $NaYF_4$:$Yb^{3+}$x%,$Ho^{3+}$1% nanoparticles (x=20, 40, 50); (d) The effect of $Yb^{3+}$ ion concentration on the intensity ratio between the red and the green UC emission. The comparison in this figure (a)-(c) was performed under identical experimental parameters of excitation and collection.

Figure 2 shows the photoluminescence spectra (from 500 to 700 nm) from the conventional $NaYF_4$:$Yb^{3+}$ x%, $Ho^{3+}$ 1% and the core-shell $NaYF_4$:$Yb^{3+}$x%@$NaYF_4$: $Ho^{3+}$ 1% UCNPs. All the conventional $NaYF_4$:$Yb^{3+}$ x%, $Ho^{3+}$ 1% UCNPs (x=20, 40, 50, 100) emit a strong green emission at ~ 540 nm and a weaker red emission at~ 650 nm (Figure 2 a). The green and red UC emissions correspond to the $^5S_2/^5F_4 \rightarrow {}^5I_8$ and the $^5F_5 \rightarrow {}^5I_8$ transitions of the $Ho^{3+}$ ions, respectively. Interestingly, the red UC emission band becomes significantly stronger than the green one in all the core-shell $NaYF_4$:$Yb^{3+}$x%@$NaYF_4$: $Ho^{3+}$ 1% UCNPs (x=20, 40, 50, 60, and 80). More clearly, as illustrated in Figure 2 d, the intensity ratio of the red/green emission ($I_{Red}/I_{Green}$) increases linearly with increasing $Yb^{3+}$ sensitizer concentration in the core-shell UCNPs, while remaining almost unchanged in the core UCNPs. In addition, when increasing the $Yb^{3+}$ concentration from 20 to 50%, the intensities of the green and red

UC emissions from the conventional UCNPs are slightly enhanced by 55% and 20%, while they are enhanced by a factor of 4 and 8.6, respectively, in the core-shell UCNPs (Figure 2c). The total integrated intensity (500-700 nm) from the core-shell $NaYF_4$:$Yb^{3+}$50%@$NaYF_4$: $Ho^{3+}$ 1% UCNPs was evaluated to be about 2 times higher than that of the conventional $NaYF_4$:$Yb^{3+}$50%, $Ho^{3+}$ 1% UCNPs. This is striking, as the $Ho^{3+}$ ions in the thin shell of the core-shell structure are supposed to manifest a pronounced surface-related quenching effect when compared to the ones located in the core UCNPs, thus generally yielding a lower UC luminescence. In all, the core-shell $NaYF_4$:$Yb^{3+}$50%@$NaYF_4$: $Ho^{3+}$ 1% UCNPs exhibit not only a tuned but also an enhanced luminescence output as compared to the conventional $NaYF_4$:$Yb^{3+}$50%, $Ho^{3+}$ 1% UCNPs (consult also Figure 4). We measured the element concentration of the resulting core-shell $NaYF_4$:$Yb^{3+}$50%@$NaYF_4$: $Ho^{3+}$ 1% with inductively coupled plasma mass spectrometry (ICP-MS), which are in general agreement with the intended theoretical values (Table S1).

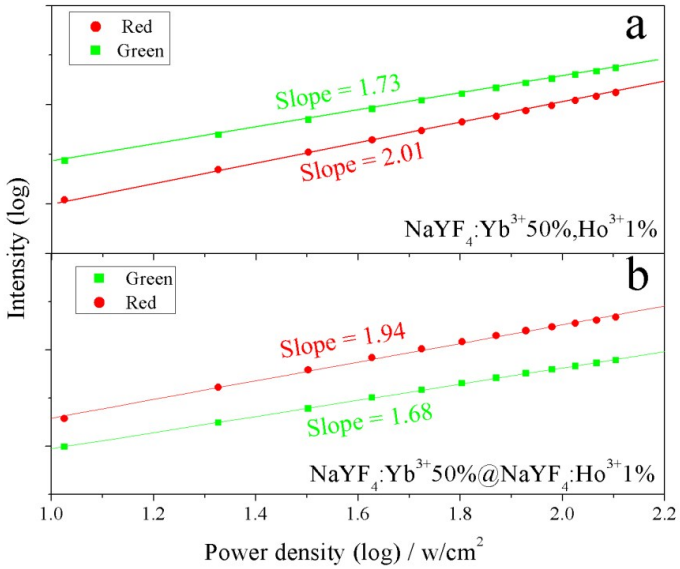


**Figure 3.** Logarithmic plot of the dependence of the intensities of the green and the red UC emission bands on the pump power for (a) the core $NaYF_4$:$Yb^{3+}$50%, $Ho^{3+}$1% and (b) the core-shell $NaYF_4$:$Yb^{3+}$50%@ $NaYF_4$:$Ho^{3+}$1% UCNPs.

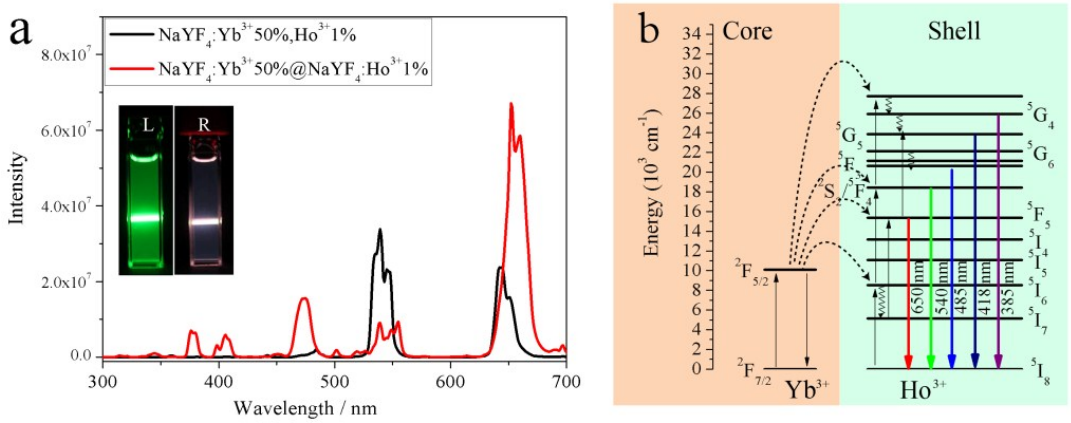


**Figure 4.** (a) Contrasted photoluminescence spectra of the conventional $NaYF_4$:$Yb^{3+}$50%,$Ho^{3+}$1% UCNPs and the core-shell $NaYF_4$:$Yb^{3+}$50%@ $NaYF_4$:$Ho^{3+}$1% UCNPs. The inset is photographic images of UC emissions of these two types of UCNPs dispersed in hexane (Left: $NaYF_4$:$Yb^{3+}$50%,$Ho^{3+}$1%, Right: $NaYF_4$:$Yb^{3+}$50%@$NaYF_4$:$Ho^{3+}$1%). The comparison was performed under identical experimental parameters of excitation and collection. (b)Energy level diagrams of the $Ho^{3+}$, $Yb^{3+}$ ions as well as the invovled UC mechanisms.

To investigate the mechanisms that result in tuned and enhanced UC in the core-shell $NaYF_4$:$Yb^{3+}$50%@$NaYF_4$: $Ho^{3+}$ 1% UCNPs, we first measured the dependence of the intensities of the green and the red UC emission band on the pump power for the conventional $NaYF_4$:$Yb^{3+}$50%, $Ho^{3+}$1% (Figure 3 a) and the core-shell $NaYF_4$:$Yb^{3+}$50%@ $NaYF_4$:$Ho^{3+}$1% (Figure 3 b) UCNPs. In general, the number of photons which are required to populate the upper emitting state under unsaturated condition can be obtained by the relation,

$$I_f \propto P^n \quad (1)$$

where $I_f$ is the photoluminescence intensity, P is the pump laser power, and n is the number of laser photons required. As one can see, the slope values for the green and the red emission bands in both the core-shell $NaYF_4$:$Yb^{3+}$50% @ $NaYF_4$:$Ho^{3+}$1% and the conventional $NaYF_4$:$Yb^{3+}$50%, $Ho^{3+}$1% UCNPs are all close to ~2. This indicates that both the green and the red emissions from the conventional and the core-shell UCNPs involve a two-photon process for their generations, in good agreement with previous results on $Yb^{3+}$/$Ho^{3+}$-codoped materials [34, 42]. Indeed, the well-established UC mechanisms for the green and the red emission involve two energy transfers from $Yb^{3+}$ ions (at its excited state) to the $Ho^{3+}$ ions, which were illustrated in detail in Figure 4 b. To gain more insights, we also carefully compared the spectra of the core-shell $NaYF_4$:$Yb^{3+}$50% @ $NaYF_4$:$Ho^{3+}$1% and the

conventional $NaYF_4$:$Yb^{3+}$50%, $Ho^{3+}$1% UCNPs in the shorter wavelength region. In addition to the observations discussed in Figure 2, there are two more noted changes: (i) the short-wavelength emissions at 385, 418, and 485 nm from the $^5G_4 \rightarrow {}^5I_8$, $^5G_5 \rightarrow {}^5I_8$, and $^5F_3 \rightarrow {}^5I_8$ transitions of $Ho^{3+}$ were greatly enhanced in the core-shell UCNPs, being ascribed to the increased excitations from the red-emitting level of the $^5F_5$ state to the $^5G_6$ or its above states (consult Figure 4 b). (ii) The shapes of emission peaks at ~540 and ~650 nm from the core-shell UCNPs vary slightly and the positions of these two peaks shift a little towards longer wavelength, in comparison to that from the conventional UCNPs. These observations indicate that the $Ho^{3+}$ ions in the shell lattice of the core-shell $NaYF_4$:$Yb^{3+}$50% @ $NaYF_4$:$Ho^{3+}$1% UCNPs experience a modified crystal field to the ones in the host lattice of the conventional $NaYF_4$:$Yb^{3+}$50%, $Ho^{3+}$1% UCNPs. Such modification of the local crystal field is liable for the increased $I_{red}/I_{green}$ ratio and an increase in the total UC emission intensity from the core-shell $NaYF_4$:$Yb^{3+}$50% @ $NaYF_4$:$Ho^{3+}$1% UCNPs. Moreover, as the core-shell $NaYF_4$:$Yb^{3+}$50% @ $NaYF_4$:$Ho^{3+}$1% UCNPs and the conventional $NaYF_4$:$Yb^{3+}$50%, $Ho^{3+}$1% UCNPs are built on the same $NaYF_4$ host lattice core, only the strain or the defect-induced strain in the shell host lattice is able to produce a perturbation on the local crystal field around the $Ho^{3+}$ ions in the core-shell UCNPs compared to the $Ho^{3+}$ ions in the conventional UCNPs.

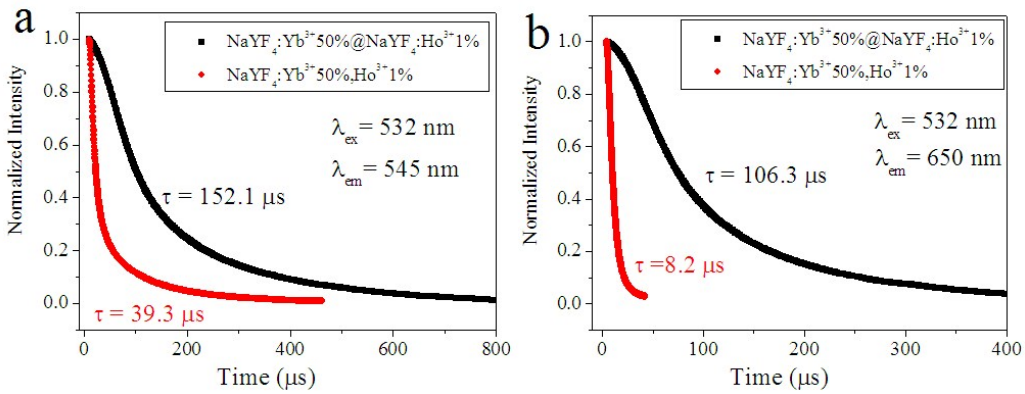


**Figure 5.** Decay profiles of (a) the transition $^5S_2/^5F_4 \rightarrow {}^5I_8$ at 545 nm and (b) the transition $^5F_5 \rightarrow {}^5I_8$ at 650 nm of $Ho^{3+}$ ions inform the conventional $NaYF_4$:$Yb^{3+}$50%, $Ho^{3+}$1% UCNPs and the core/shell $NaYF_4$:$Yb^{3+}$50%@ $NaYF_4$:$Ho^{3+}$1% UCNPs.

To verify that the increased $I_{red}/I_{green}$ ratio and the enhanced UC emission intensity in the core-shell UCNPs arise from the effect of modified local crystal field, the decay profiles of

the transition $^5S_2/^5F_4 \rightarrow {}^5I_8$ of $Ho^{3+}$ ions at 545 nm and the transition $^5F_5 \rightarrow {}^5I_8$ of $Ho^{3+}$ ions at 650 nm from both the conventional $NaYF_4$:$Yb^{3+}$50%, $Ho^{3+}$1% nanoparticles and the core/shell $NaYF_4$:$Yb^{3+}$50%@$NaYF_4$:$Ho^{3+}$1% nanoparticles were measured and shown in Figure 5. The measured decay curves in general are non- exponential due to enhanced nonradiative energy transfer processes as well as from the effect of surrounding environment [43]. The effective lifetime $\tau_m$ was evaluated to analyze the decay process, using the following equation:

$$\tau_m = \frac{\int_0^{+\infty} tI(t)dt}{\int_0^{+\infty} I(t)dt} \quad (2)$$

where $I$(t) is the intensity at time t. The effective decay times for the $^5S_2/^5F_4$ and $^5F_5$ state are evaluated to be about 39.3 and 8.2 μs for the conventional UCNPs, and 152.1 and 106.3 μs for the core-shell UCNPs, respectively. The $Ho^{3+}$ ions in the thin shell (~2 nm) of the core-shell UCNPs are more susceptible to experience surface-related quenching effect than the ones in the core UCNPs do, as they are more close to the surrounding environment. As a consequence, the effective lifetimes in the core-shell $NaYF_4$:$Yb^{3+}$50% @ $NaYF_4$:$Ho^{3+}$1% UCNPs are supposed to be shorter than the ones in the core $NaYF_4$:$Yb^{3+}$50%, $Ho^{3+}$1% UCNPs. However, a prolonged lifetime is experimentally observed for the core-shell UCNPs, substantiating that the optical transition parameters of $Ho^{3+}$ indeed are changed by strain-induced modification of the local crystal field.

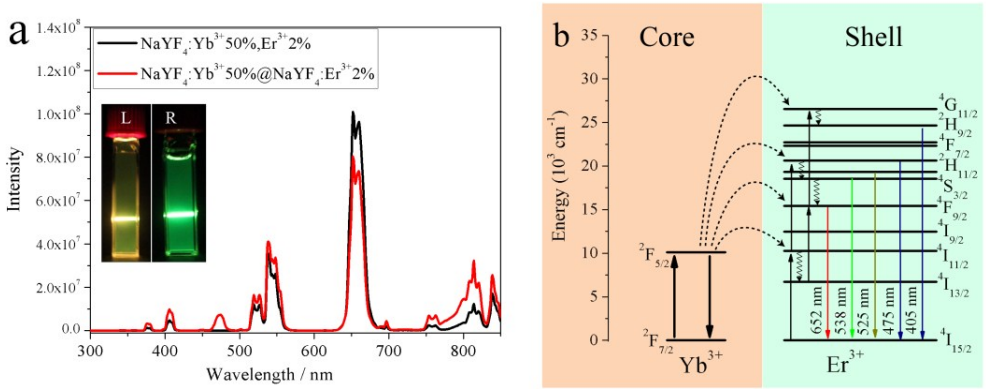


**Figure 6**. (a) Comparison of the photoluminescence spectrum of $NaYF_4$:$Yb^{3+}$50%,$Er^{3+}$2% nanoparticles and $NaYF_4$:$Yb^{3+}$50%@ $NaYF_4$: $Er^{3+}$2% nanoparticles. Inset is the luminescence photographs of the nanoparticles dispersed in hexane (Left: $NaYF_4$:$Yb^{3+}$50%, $Er^{3+}$2%, Right: $NaYF_4$:$Yb^{3+}$50%@$NaYF_4$:$Er^{3+}$2%). The comparison was performed under identical experimental parameters of excitation and collection. (b) Energy level diagrams of $Er^{3+}$, $Yb^{3+}$ ions as well as involved UC mechanisms

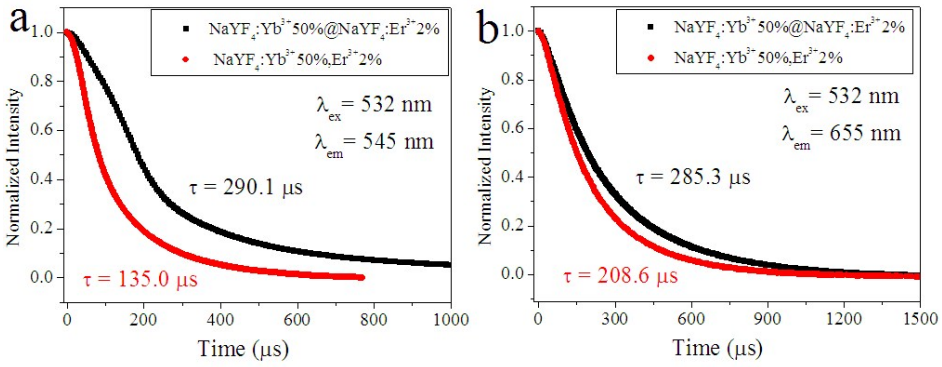


**Figure 7.** Decay profiles of (a) the transition $^4S_{3/2}\rightarrow {}^4I_{15/2}$ at 545 nm and (b) the transition $^4F_{9/2}\rightarrow {}^4I_{15/2}$ at 655 nm, of $Er^{3+}$ ions from the conventional $NaYF_4$:$Yb^{3+}$50%,$Er^{3+}$2% nanoparticles and the core/shell $NaYF_4$:$Yb^{3+}$50%@ $NaYF_4$: $Er^{3+}$2% UCNPs.

We also prepared the core-shell $NaYF_4$:$Yb^{3+}$50%@$NaYF_4$:$Er^{3+}$2% and its corresponding conventional $NaYF_4$:$Yb^{3+}$50%, $Er^{3+}$2% UCNPs, as well as the core-shell $NaYF_4$:$Yb^{3+}$50%@$NaYF_4$:$Tm^{3+}$1% and its corresponding conventional $NaYF_4$:$Yb^{3+}$50%, $Tm^{3+}$1% UCNPs. We measured the element concentration of the resulting core-shell $NaYF_4$:$Yb^{3+}$50%@$NaYF_4$:$Er^{3+}$2% with ICP-MS, which are in general agreement with the intended theoretical values (Table S2). Figure 6 (a) and its inset illustrate that the yellowish UC emission (appeared to the naked eyes) from the conventional $NaYF_4$:$Yb^{3+}$50%, $Er^{3+}$2% UCNPs is converted into the green UC emission. This is mainly because the intensity ratio between the green emission 545 nm ($^4S_{3/2}\rightarrow {}^4I_{15/2}$) and the red emission at 655 nm ($^4F_{9/2}\rightarrow {}^4I_{15/2}$) of $Er^{3+}$ ions is increased in the core-shell structure compared to the conventional UCNPs. The UC mechanisms to populate the green and the red emission of $Er^{3+}$ are depicted in Figure 6 (b). The branch ratio of the $^4S_{3/2}$ state for the $^4S_{3/2}\rightarrow {}^4I_{13/2}$ transition (~800 nm) to the $^4S_{3/2}\rightarrow {}^4I_{15/2}$ transition (~ 540 nm) can be determined by the corresponding emission intensity ratio of $I_{800}/I_{540}$. This value in principle should be a fixed one for the conventional and the core-shell UCNPs, as they both utilize the same hexagonal $NaYF_4$ material as the host lattice. However, this branch ratio is increased from 1.4 for the conventional $NaYF_4$:$Yb^{3+}$50%, $Er^{3+}$2% UCNPs, to 2.9 for the core-shell $NaYF_4$:$Yb^{3+}$50%@$NaYF_4$:$Er^{3+}$2% UCNPs. In addition, similar to the observations in Figure 5, the decay rates for the green and red emissions of $Er^{3+}$ were slower in the core-shell structure as compared to the conventional one (Figure 7). The increased branch ratio of the $^4S_{3/2}$ state as well as the observed prolonged lifetimes again confirm the presence of strain-induced modification of the local crystal field in the shell host

lattice. Moreover, the prolonged lifetimes in the core-shell $NaYF_4$:$Yb^{3+}$50%@$NaYF_4$:$Er^{3+}$2% UCNPs also correlate with an increase of the total UC emission intensity when comparing them with that of the conventional $NaYF_4$:50%$Yb^{3+}$,1%$Er^{3+}$ UCNPs.

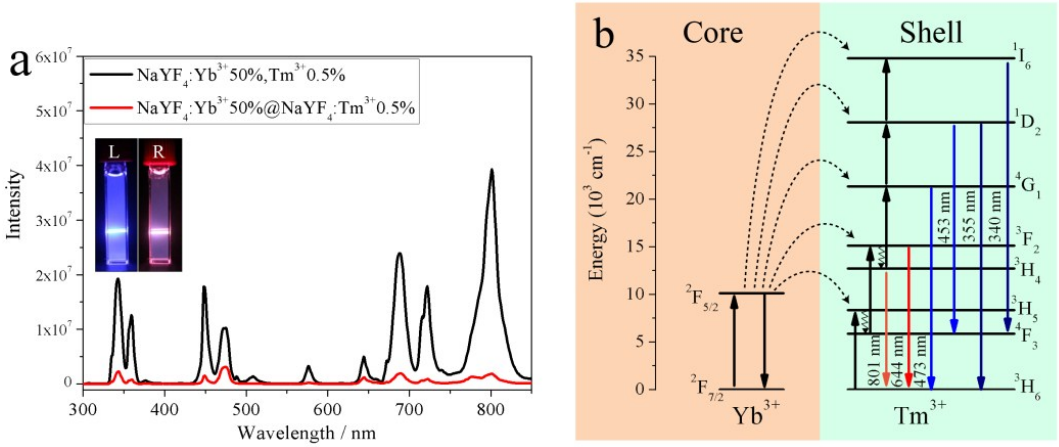


**Figure 8.** (a) Contrasted photoluminescence spectrum of the $NaYF_4$:$Yb^{3+}$50%,$Tm^{3+}$1% UCNPs and the core-shell $NaYF_4$:$Yb^{3+}$50%@ $NaYF_4$: $Tm^{3+}$1% UCNPs. The inset is a photoographic image of UC emissions from these two types of UCNPs dispersed in hexane. (Left: $NaYF_4$:$Yb^{3+}$50%, $Er^{3+}$2%, Right: $NaYF_4$:$Yb^{3+}$50%@$NaYF_4$:$Er^{3+}$2%). The comparison was performed under identical experimental parameters of excitation and collection. (b) Energy level diagrams of $Tm^{3+}$, $Yb^{3+}$ ions as well as the involved UC mechanisms. Step-wise energy transfers from the $Yb^{3+}$ to the $Tm^{3+}$ is responsive for populating the pertinent emitting energy level.

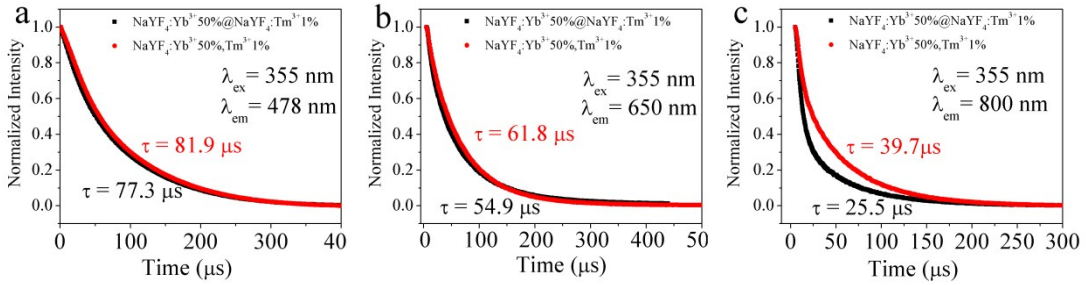


**Figure 9.** Decay profiles of (a) the transition $^4G_1$→ $^3H_6$ at 478 nm, (b) the transition $^3F_2$→ $^3H_6$, and (c) the transition $^3H_4$→ $^3H_6$ at 655 nm, of $Tm^{3+}$ ions from the $NaYF_4$:$Yb^{3+}$50%, $Tm^{3+}$1% UCNPs and core/shell $NaYF_4$:$Yb^{3+}$50%@ $NaYF_4$: $Tm^{3+}$2% UCNPs.

The classic blue color output of the UC emission from the $NaYF_4$:$Yb^{3+}$50%, $Tm^{3+}$1% UCNPs was converted into the pink blue color output from the core-shell $NaYF_4$:$Yb^{3+}$50%@$NaYF_4$:$Tm^{3+}$1% UCNPs (Figure 8 and its inset). Moreover, the relative intensities of UV UC emissions at 340/355 nm (five/four-photon process) and blue UC emissions at 455/473 nm (four/three-photon process) to the intensity of NIR UC emission at

800 nm (two-photon process), are both increased a lot when utilizing the core-shell structure. This indicates that higher order multi-photon processes are favored by the core-shell structure, despite with a diminution of the total UC luminescence intensity. We measured the element concentration of the resulting core-shell $NaYF_4$:$Yb^{3+}$50%@$NaYF_4$:$Tm^{3+}$1% with ICP-MS, which are in general agreement with the intended theoretical values (Table S3). The variance of visualized color as well as the redistribution of upconverted energy in different bands illustrates that the $NaYF_4$:$Yb^{3+}$ @$NaYF_4$:$RE^{3+}$ core-shell structure are able to tune the color output of the typically used $NaYF_4$:$Yb^{3+}$/$RE^{3+}$ UCNPs. The mechanisms for generating UC emission peaks of $Tm^{3+}$ have been well-established, which are depicted in Figure 8(b). Unlike the $NaYF_4$:50%$Yb^{3+}$@$NaYF_4$:2%$Ho^{3+}$ and $NaYF_4$:50%$Yb^{3+}$ @$NaYF_4$:2%$Er^{3+}$ core-shell UCNPs, the $NaYF_4$:50%$Yb^{3+}$ @$NaYF_4$:1%$Tm^{3+}$ core-shell form presents a very slightly shorter effective decay times than the conventional $NaYF_4$:50%$Yb^{3+}$,1%$Tm^{3+}$ UCNPs (Figure 9). This corresponds to a decrease in the total UC emission intensity from the core-shell $NaYF_4$:50%$Yb^{3+}$ @$NaYF_4$:1%$Tm^{3+}$ UCNPs than from the conventional $NaYF_4$:50%$Yb^{3+}$, 1%$Tm^{3+}$ UCNPs. This experimental fact indicates that the strain-induced modification of the crystal filed in the shell of the $NaYF_4$:$Yb^{3+}$ @$NaYF_4$:$RE^{3+}$ core-shell UCNPs manifest different luminescence intensity change for different activator $RE^{3+}$ ions (consult also Figures 4 a and 6a for the case of RE = Ho and RE = Er). In addition, we would like to point out that the conservation of relatively high upconversion efficiency nature in sensitizer-activator-isolated UCNP lies in efficacious energy migrations within $Yb^{3+}$ sub-lattice in the core to the activator ions located in the shell. The two-energy-level system of $Yb^{3+}$ ion as well as its long lifetime of excited states enables the excitation energy to migrate efficiently and randomly throughout the core nanoparticles with very limited energy losses.[16-18] This migrated energy can then cross the interface between the core and the shell layer to excite those activators that are closely located at the interface due to the spatial confinement of the thin shell layer, thus producing upconversion at a relatively high efficiency.

## Conclusion

We have demonstrated the optical emission pathways of the activator $RE^{3+}$(RE=Ho, Er,

Tm) in the $NaYF_4:Yb^{3+}$@$NaYF_4:RE^{3+}$ core-shell structure vary from that of the typically used $NaYF_4:Yb^{3+}/RE^{3+}$ conventional UCNPs. This results in a quasi-white, green, and pink blue UC color output from the core-shell $NaYF_4:Yb^{3+}$ @$NaYF_4:Ho^{3+}$, $NaYF_4:Yb^{3+}$ @$NaYF_4:Er^{3+}$, and $NaYF_4:Yb^{3+}$ @$NaYF_4:Tm^{3+}$ UCNPs, in marked contrast to the green, yellow, and pure blue output from the corresponding conventional $NaYF_4:Yb^{3+}/RE^{3+}$ nanoformulation. The strain-induced modulation of the shell crystal field is liable for the modification of optical emission channels, which is supported by the time-resolved spectra. This work provides a new paradigm for tuning UC emission color output, having implications for a range of biophotonic and other photonic applications.

## Acknowledgements.

This work has been partially supported by the National Basic Research Program of China (Grant No. 2015CB352005, 2012CB825802), National Natural Science Foundation of China (61378091, 61405123, and 51102066), the Program for the Basic Research Excellent Talents of Harbin Institute of Technology (No. BRETIII 2012018), and the Fundamental Research Funds for the Central Universities (Grant No. HIT. AUGA5710052614). We thank Ms. Jossana Damasco for her assistance in inductively coupled plasma mass spectrometry (ICP-MS) measurement.

## References


1. S. Gai, C. Li, P. Yang, J. Lin. Recent progress in rare earth micro/nanocrystals: soft chemical synthesis, luminescent properties, and biomedical applications. Chem. Rev. 2014, 114, 2343−2389
2. F. Wang, Y. Han, C. S. Lim, Y. Lu, J. Wang, J. Xu, H. Chen, C. Zhang, M. Hong, X. Liu. Simultaneous phase and size control of upconversion nanocrystals through lanthanide doping, Nature, 2010, 463, 1061-1065
3. G. Wang, Q. Peng, Y. Li. Lanthanide doped nanocrystals: synthesis, optical-magnetic properties, and applications, Accounts of Chemical Research, 2011, 44, 322–332
4. J. Shen, L. Zhao, G. Han. Lanthanide-doped upconverting luminescent nanoparticle platforms for optical imaging-guided drug delivery and therapy, Advanced Drug Delivery Reviews, 2013, 65, 744–755
5. G. Chen, J. Seo, C. Yang, P. N. Prasad. Nanochemistry and nanomaterials for photovoltaics, Chem. Soc. Rev., 2013, 42, 8304—8338
6. C. Yuan, G. Chen, L. Li, J.A. Damasco, Z. Ning, H. Xing, T. Zhang, L. Sun, H. Zeng, A. N. Cartwright, P. Prasad, Hans Agren. Simultaneous multiple wavelength upconversion in a core−shell nanoparticle for enhanced near infrared light harvesting in a dye-sensitized solar cell, ACS Appl. Mater. Interfaces 2014, 6, 18018−18025
7. L. Zhou, Z. Li, Z. Liu, M. Yin, J. Ren, X. Qu. One-step nucleotide-programmed growth of porous upconversion nanoparticles: application to cell labeling and drug delivery, Nanoscale, 2014, 6, 1445–1452
8. Y. Liu, D. Tu, H. Zhu, E. Maa, X. Chen. Lanthanide-doped luminescent nano-bioprobes: from fundamentals to biodetection, Nanoscale, 2013, 5, 1369–1384
9. G. Chen, T. Y. Ohulchanskyy, S. Liu, W. C. Law, F. Wu, M. T. Swihart, H. Agren, P. N. Prasad. Core/shell $NaGdF_4:Nd^{3+}/NaGdF_4$ nanocrystals with efficient near-infrared to near-infrared downconversion photoluminescence for bioimaging applications, ACS Nano, 2012, 6, 2969-2977
10. Y. Zhou, S.T. Han, X. Chen, F. Wang, Y. B. Tang, V. Roy. An upconverted photonic nonvolatile memory, Nat. Commun., 2014, 5, 1-8

11. J Liu, W Bu, L Pan, J Shi. NIR-Triggered Anticancer Drug Delivery by Upconverting Nanoparticles with Integrated Azobenzene-Modified Mesoporous Silica, Angew. Chem. Int. Ed. 2013, 52, 4375–4379
12. W Fan, B Shen, W Bu, F Chen, Q He, K Zhao, S Zhang, L Zhou, W Peng, Q Xiao, D Ni, J Liu, J Shi. A smart upconversion-based mesoporous silica anotheranostic system for synergetic chemo-/radio-/photodynamic therapy and simultaneous MR/UCL imaging, Biomaterials, 2014, 35, 8992-9002
13. K. Koenig. Multiphoton microscopy in life sciences, Journal of Microscopy, 2000, 200, 83-104
14. X. Yu, L. Chen, M. Li, M. Xie, L. Zhou, Y. Li, Q. Wang. Highly efficient fluorescence of $NdF_3/SiO_2$ Core/Shell nanoparticles and the Applications for in vivo NIR detection, Adv. Mater. 2008, 20, 4118–4123
15. A. Xia, M. Chen, Y. Gao, D. Wu, W. Feng, F. Li. $Gd^{3+}$ complex-modified $NaLuF_4$-based upconversion nanophosphors for trimodality imaging of NIR-to-NIR upconversion luminescence, X-Ray computed tomography and magnetic resonance, Biomaterials, 2012, 33, 5394e5405
16. G. Chen, C. Yang, P. N. Prasad. Nanophotonics and Nanochemistry: Controlling the Excitation Dynamics for Frequency Up- and Down-Conversion in Lanthanide-Doped Nanoparticles, Accounts of Chemical Research, 2013, 46, 1474–1486
17. G. Chen, H. Ågren, T. Y. Ohulchanskyya, P. N. Prasad. Light upconverting core–shell nanostructures: nanophotonic control for emerging applications, Chem. Soc. Rev., 2015, DOI: 10.1039/c4cs00170b
18. G. Chen, H. Qiu, P. N. Prasad, X. Chen. Upconversion nanoparticles: design, nanochemistry, and applications in theranostics, Chem. Rev. 2014, 114, 5161−5214
19. G. Chen, H. Qiu, R. Fan, S. Hao, S. Tan, C. Yang, G. Han. Lanthanide-doped ultrasmall yttrium fluoride nanoparticles with enhanced multicolor upconversion photoluminescence, J. Mater. Chem., 2012, 22, 20190–20196
20. J. Boyer, F. Vetrone, L. A. Cuccia, J. A. Capobianco. Synthesis of colloidal upconverting $NaYF_4$ nanocrystals doped with $Er^{3+}$, $Yb^{3+}$ and $Tm^{3+}$, $Yb^{3+}$ via thermal decomposition of lanthanide trifluoroacetate precursors, J. Am. Chen. Soc. 2006, 128, 7444-7445

21. S. Heer, K. Kompe, H. U. Gudel, M. Haase. Highly efficient multicolour upconversion emission in transparent colloids of lanthanide doped $NaYF_4$ nanocrystals, Adv. Mater. 2004, 16, 2012-2015

22. H. Mai, Y. Zhang, L. Sun, C. Yan. Highly efficient multicolor Upconversion emissions and their mechanisms of monodisperse $NaYF_4$:Yb,Er Core and Core/Shell-structured nanocrystals, J. Phys. Chem. C, 2007, 111, 13721-13729

23. A. Punjabi, X. Wu, A. Tokatli-Apollon, M. El-Rifai, H. Lee, Y. Zhang, C. Wang, Z. Liu, E. M. Chan, C. Duan, G. Han. Amplifying the red-emission of upconverting nanoparticles for biocompatible clinically used prodrug-induced photodynamic therapy, ACS Nano, 2014, 8, 10621-10630

24. J. Shen , G. Chen , T. Y. Ohulchanskyy , S. J. Kesseli , S. Buchholz , Z. Li , P. N. Prasad , G. Han. Tunable near infrared to ultraviolet upconversion luminescence enhancement in ($\alpha$-$NaYF_4$:Yb,Tm)/$CaF_2$ core/shell nanoparticles for in situ real-time recorded biocompatible photoactivation, small, 2013, 9, 3213–3217

25. W. Wei, Y. Zhang, R. Chen, J. Goggi, N. Ren, L. Huang, K. K. Bhakoo, H. Sun, T. T. Yang Tan. Cross relaxation induced pure red upconversion in activator- and sensitizer-rich lanthanide nanoparticles, Chem. Mater. 2014, 26, 5183−5186

26. H. Qian, Y. Zhang. Synthesis of Hexagonal-phase core-shell $NaYF_4$ nanocrystals with tunable upconversion fluorescence, Langmuir 2008, 24, 12123-12125

27. Q. Dou, N. M. Idris, Y. Zhang. Sandwich-structured upconversion nanoparticles with tunable color for multiplexed cell labeling, Biomaterials, 2013, 34, 1722-1731

28. F. Wang, X. Liu. Upconversion multicolor fine-tuning: visible to near-infrared emission from lanthanide doped $NaYF_4$ nanoparticles, J. Am. Chem. Soc. 2008, 130, 5642–5643

29. G. Tian, Z. Gu, L. Zhou, W. Yin, X. Liu, L. Yan, S. Jin, W. Ren, G. Xing, S. Li, Y. Zhao. $Mn^{2+}$ dopant-controlled synthesis of $NaYF_4$:Yb/Er upconversion nanoparticles for in vivo imaging and drug delivery, Adv. Mater. 2012, 24, 1226–1231

30. H. Wang, W. Lu, Z. Yi, L. Rao, S. Zeng, Z. Li. Enhanced upconversion luminescence and single-band red emission of $NaErF_4$ nanocrystals via $Mn^{2+}$ doping, Journal of Alloys and Compounds, 2015, 618, 776–780

31. J. Wang, F. Wang, C. Wang, Z. Liu, X. Liu. Single band upconversion emission in

lanthanide doped $KMnF_3$ nanocrystals, Angew. Chem. Int. Ed., 2011, 50, 10369 –10372

32. D. Chen, L, Lei, R. Zhang, A. Yang, J. Xu, Y. Wang. Intrinsic single-band upconversion emission in colloidal Yb/Er(Tm):$Na_3Zr(Hf)F_7$ nanocrystals, Chem. Commun., 2012, 48, 10630–10632
33. W. Gao, H. Zheng, Q. Han, E. He, F. Gao, R. Wang. Enhanced red upconversion luminescence by codoping $Ce^{3+}$ in β-$NaY(Gd_{0.4})F_4$:$Yb^{3+}$/$Ho^{3+}$ nanocrystals, J. Mater. Chem. C, 2014, 2, 5327–5334
34. G. Chen, H. Liu, G. Somesfalean, H. Liang, Z. Zhang. Upconversion emission tuning from green to red in $Yb^{3+}$/$Ho^{3+}$-codoped $NaYF_4$ nanocrystals by tridoping with $Ce^{3+}$ ions, Nanotechnology, 2009, 20, 385704
35. W. Niu, S. Wu, S. Zhang. Utilizing the amidation reaction to address the ‘‘cooperative effect’’ of carboxylic acid/amine on the size, shape, and multicolor output of fluoride upconversion nanoparticles, J. Mater. Chem., 2011, 21, 10894-10902
36. W. Niu, S. Wu, S. Zhang. A facile and general approach for the multicolor tuning of lanthanide ion doped $NaYF_4$ upconversion nanoparticles within a fixed composition, J. Mater. Chem., 2010, 20, 9113–9117
37. X. Ye, J. E. Collinsb, Y. Kanga, J.n Chenc, D. T. N. Chend, A. G. Yodhd, C. B. Murray. Morphologically controlled synthesis of colloidal upconversion nanophosphors and their shape-directed self-assembly, PNAS, 2010, 107, 22430–22435
38. F. Wang, J. Wang, X. Liu. Direct evidence of a surface quenching effect on size-dependent luminescence of upconversion nanoparticles, Angew. Chem. Int. Ed. 2010, 49, 7456 –7460
39. Z. Li, Y. Zhang. An efficient and user-friendly method for the synthesis of hexagonal-phase $NaYF_4$:Yb, Er/Tm nanocrystals with controllable shape and upconversion fluorescence, Nanotechnology, 2008, 19, 345606
40. W. Shao, G. Chen, T. Y. Ohulchanskyy, A. Kuzmin, J. Damasco, H. Qiu, C. Yang, H. Agren, P. N. Prasad. Lanthanide doped fluoride core/multishell nanoparticles for broadband upconversion of infrared light, Adv. Optical. Mater., 2014, 2, DOI:

10.1002/adom.201400404

41. J. A. Damasco, G. Chen, W. Shao, H. Ågren, H. Huang, W. Song, J. F. Lovell, P. N. Prasad. Size-tunable and monodisperse $Tm^{3+}/Gd^{3+}$ doped hexagonal $NaYbF_4$ nanoparticles with engineered efficient near infrared-to-near infrared upconversion for in vivo imaging, ACS Appl. Mater. Interfaces, 2014, 6, 13884−13893
42. G. Chen, C. Yang, B. Aghahadi, H. Liang, Y. liu, L. Li, and Z. Zhang. Ultraviolet-blue upconversion emission of $Ho^{3+}$ ions. J. Opt. Soc. Am. B 2010, 27, 1158-1164.
43. F. Pandozzi, F. Vetrone, J. Boyer, R. Naccache, J. A. Capobianco, A. Speghini, M. Bettinelli. A spectroscopic analysis of blue and ultraviolet upconverted emissions from $Gd_3Ga_5O_{12}:Tm^{3+}$, $Yb^{3+}$ nanocrystals, J. Phys. Chem. B 2005, 109, 17400-17405